Neuro-Oncology 12(9):928–940, 2010.
doi:10.1093/neuonc/noq046
Advance Access publication May 20, 2010

Canine spontaneous glioma: A translational model system for convection-enhanced delivery

Peter J. Dickinson, Richard A. LeCouteur, Robert J. Higgins, John R. Bringas, Richard F. Larson, Yoji Yamashita, Michal T. Krauze, John Forsayeth, Charles O. Noble, Daryl C. Drummond, Dmitri B. Kirpotin, John W. Park, Mitchel S. Berger, and Krystof S. Bankiewicz

Departments of Surgical and Radiological Sciences (P.J.D., R.A.L., R.F.L.), Pathology, Microbiology, and Immunology (R.J.H.), School of Veterinary Medicine, University of California–Davis, Davis, California; Department of Neurosurgery, Brain Tumor Research Center (J.R.B., Y.Y., M.T.K., J.F., M.S.B., K.S.B.) and Division of Hematology-Oncology (C.O.N., J.W.P.), University of California–San Francisco, San Francisco, California; Merrimack Pharmaceuticals, Cambridge, Massachusetts (C.O.N., D.C.D., D.B.K.)

Canine spontaneous intracranial tumors bear striking similarities to their human tumor counterparts and have the potential to provide a large animal model system for more realistic validation of novel therapies typically developed in small rodent models. We used spontaneously occurring canine gliomas to investigate the use of convection-enhanced delivery (CED) of liposomal nanoparticles, containing topoisomerase inhibitor CPT-11. To facilitate visualization of intratumoral infusions by real-time magnetic resonance imaging (MRI), we included identically formulated liposomes loaded with Gadoteridol. Real-time MRI defined distribution of infusate within both tumor and normal brain tissues. The most important limiting factor for volume of distribution within tumor tissue was the leakage of infusate into ventricular or subarachnoid spaces. Decreased tumor volume, tumor necrosis, and modulation of tumor phenotype correlated with volume of distribution of infusate (Vd), infusion location, and leakage as determined by real-time MRI and histopathology. This study demonstrates the potential for canine spontaneous gliomas as a model system for the validation and development of novel therapeutic strategies for human brain tumors. Data obtained from infusions monitored in real time in a large, spontaneous tumor may provide information, allowing more accurate prediction and optimization of infusion parameters. Variability in Vd between tumors strongly suggests that real-time imaging should be an essential component of CED therapeutic trials to allow minimization of inappropriate infusions and accurate assessment of clinical outcomes.

Keywords: brain tumors, canine, CPT-11, convection-enhanced delivery, magnetic resonance imaging.

The long-term prognosis for patients with malignant gliomas after conventional therapy is poor, and has remained relatively static over the last 30 years. Many novel strategies have been developed for the treatment of malignant gliomas; however, few have progressed beyond early-phase clinical trials. One of the major reasons for the failure to reproduce the dramatic results seen in preclinical therapeutic development is the large "translational distance" between spontaneous, large invasive tumors in people, and the classical immunologically compromised, small, clonal, rodent xenograft tumor model systems typically used in preclinical development and testing. Recent development of transgenic models of glioma promise to provide a more realistic testing ground, at least at the molecular level,[1] and some characterized orthotopic rodent models have been shown to mimic clinical reality relating to therapeutic issues such as 1p19q status and the use of surgery and chemotherapy combinations.[2] However, the significant limitations of rodent models, particularly

Received October 28, 2009; accepted March 15, 2010.

Corresponding Author: Peter J. Dickinson, PhD, BVSc, Department of Surgical and Radiological of Sciences, UC Davis School of Veterinary, One Shields Avenue, 2112 Tupper Hall, Davis, CA 95616-8745 (pjdickinson@ucdavis.edu).

relating to the mechanistics of delivery and tumor heterogeneity, remain.

Naturally occurring cancers in pet dogs, including tumors of the nervous system, are as diverse as the cancers seen in humans and have many similarities to their human tumor counterparts.[3,4] Specific cancers are often overrepresented in certain breeds, within which exists a limited degree of genetic variation. This homogeneity provides an ideal background for the identification of underlying genetic abnormalities. A number of factors make canine cancers attractive from a drug development vantage. These include the relatively rapid cancer progression rates relative to humans, and the opportunity to treat over long periods of time (relative to rodent models), in "large" spontaneous tumors that exhibit both heterogeneity and genomic instability. All these factors together may provide a rapid and more realistic approach to preclinical therapeutic assessment of novel strategies developed and proven in rodent model systems.[5,6]

The incidence of primary brain and central nervous system (CNS) tumors in humans is approximately 6–12 of 100 000 person-years,[7,8] with a necropsy frequency of brain tumors of approximately 2%.[9] Although the true incidence of canine gliomas is unknown, the frequency of brain tumors in dogs, based on necropsy data, is similar to humans (ie, approximately 3%), with primary intracranial tumors accounting for approximately 2%.[10] The prevalence of nervous system tumors in the general population of pet dogs is also similar and has been estimated at 14.5 of 100 000 animal-years.[11,12] In addition to the similar frequency of occurrence, a parallel spectrum of canine tumor types arise that bear striking similarities to their human tumor counterparts in terms of histopathology[4,13–18] and neuroimaging.[16,18–22] Molecular and cytogenetic characterization of canine primary brain tumors, though preliminary, is advancing rapidly since the publication of the canine genome. Many similarities to human tumors have already been described, relating to chromosomal instability, expression profiles, the presence of stem-like tumor cells, expression of growth factors and their receptors such as EGF, PDGF, VEGF, as well as other markers frequently described in human tumors such as IL-13Rα2, IGFBP2, and telomerase activity.[17,22–31] Limited data are available relating to the efficacy of standard therapeutic modalities in canine gliomas, and it is likely that some significant differences will be present between human and canine gliomas, as has already been described for meningiomas.[30,32] However, as the number of molecular similarities are further defined, spontaneous canine tumors, with their relatively large size and heterogeneous nature, are becoming attractive for translational investigation of both targeted and nontargeted novel therapies in a tumor environment more representative of the human clinical situation.

Convection-enhanced delivery (CED) of therapeutic agents into brain is a promising treatment strategy, allowing direct infusion of high concentrations of therapeutic drugs, while essentially eliminating systemic toxicity.[33] However, our current inability to accurately define the extent and location of infusions in real-time considerably limits the therapeutic efficacy at the individual level, and reduces our ability to objectively assess the outcome in clinical trials. CPT-11 (Irinotecan) is a water-soluble derivative of the potent alkaloid anticancer agent camptothecin and acts as a specific inhibitor of topoisomerase I.[34] It has been shown to be one of the most active agents against a variety of CNS xenograft tumors when delivered systemically.[35] On the basis of this experimental data, CPT-11 has progressed into clinical trials for a variety of primary brain tumors either alone or in combination therapies.[36] Because prognosis for canine intra-axial gliomas is generally poor with conventional therapy, we surmised that these tumors might provide a valuable translational model system to investigate the value of real-time MRI during intratumoral CED of novel therapeutic agents in a realistic large animal model system. We show here that CED of liposomal nanoparticles containing the topoisomerase I inhibitor CPT-11 and the surrogate marker Gadoteridol into spontaneously occurring, nonresected gliomas is feasible and potentially efficacious. Moreover, efficacy defined by decreased tumor volume and modulation of tumor phenotype correlated with volume of distribution of infusate (Vd), cannula location, and leakage of infusate as revealed by real-time magnetic resonance imaging (MRI). These data suggest that real-time imaging should be an essential component of CED therapeutic trials and that intratumoral CED may offer additional therapeutic options for nonresectable tumors. Further study of CED in canine spontaneous gliomas correlating infusion characteristics with real-time imaging and histopathology is likely to provide valuable data for the optimization of CED, as well as preliminary assessment of the efficacy and safety of novel therapeutic drugs.

Materials and Methods

Clinical Patients

Dogs receiving CED of liposomal CPT-11 were patients at the Veterinary Medical Teaching Hospital (VMTH), School of Veterinary Medicine, University of California, Davis. The clinical trial was reviewed and approved by the Institutional Animal Care and Use Committee (IACUC) at the University of California, Davis, and by the VMTH clinical trials review board. All dogs had spontaneous intra-axial gliomas confirmed histopathologically by stereotactic CT-guided biopsy. Dogs were considered suitable candidates for treatment if they had minimal neurological deficits at the time of presentation and tumors were located rostro-tentorially, involving either the cerebrum or thalamus. Complete blood counts, serum biochemical analyses, and cerebrospinal fluid (CSF) analyses were acquired from all animals immediately prior to the CED procedures, and at scheduled follow-up MRI after infusions. Blood samples were collected via jugular puncture and CSF was taken via cerebellomedullary cisternal puncture (under general anesthesia). CSF was analyzed for cellular

and total protein content within 30 minutes of collection. Animals were monitored throughout the clinical trial period by serial neurological examination and serial MRI.

Liposome Preparation

Separate liposomes were prepared for detection by MRI and for delivery of CPT-11. Gadoteridol (Gd) was obtained commercially as 0.5 M 10-(2-hydroxy-propyl)-1,4,7,10-tetraazacyclododecane-1,4,7-triacetic acid (Prohance; Bracco Diagnostics, Princeton, New Jersey). Liposome-encapsulated gadolinium (GDL) was prepared as described previously.[37,38] Briefly, the lipids were hydrated in Prohance followed by extrusion 5 times through a 0.2 μm polycarbonate membrane then 8 times through a 0.1-μm polycarbonate membrane. Unencapsulated gadoteridol was removed by purification on a Sephadex G-75 size-exclusion column eluted with HEPES-buffered saline (pH 7.25). The resulting GDL had a diameter ranging from 93.6 to 108 nm as determined by quasi-elastic light scattering (N4Plus particle size analyzer, Beckman Coulter, Fullerton, Louisiana) and was sterilized by passage through a 0.2-μm polyethersulphone (PES) syringe filter. CPT-11 (gift from PharmaEngine, Inc., Taipei, Taiwan) was loaded into liposomes composed of 1,2-distearoyl-*sn*-glycero-3-phosphocholine, cholesterol, and 1,2-distearoyl-*sn*-glycero-3-phosphoethanolamine-*N*-[methoxy(polyethylene glycol)-2000] (PEG–DSPE) at the molar ratio of 3:2:0.015 with the drug-trapping agent triethylammonium sucrose octasulphate (TEA-SOS), as described previously.[39] CPT-11 HCl was incubated with TEA-SOS containing liposomes at 60°C (pH 6.0) for 45 minutes followed by quenching on ice for 15 minutes. Unencapsulated CPT-11 was removed by Sephadex G75 size-exclusion chromatography, and the liposomal CPT-11 was concentrated on a stirred cell concentrator containing a regenerated cellulose 1×10^5 NMWL membrane (Amicon, Millipore Corp., Billerica, Massachusetts) and sterilized by passage through a 0.2-μm PES syringe filter. The CPT-11 concentration was determined by measuring the absorbance at 375 nm of a solubilized sample. The final formulation contained nanoliposomal CPT-11 with the potency equivalent to 45 mg/mL CPT-11 HCl and nanoliposomal Gadoteridol with the potency equivalent to 2.0 mM Gadoteridol.

MRI Acquisition

Transverse T1- and T2-weighted images of the dogs' brains were acquired with animals secured in a stereotactic head frame. A 1.5T Signa LX scanner (GE Medical Systems, Waukesha, Wisconsin) and 5″ circular surface coil were used to obtain baseline spoiled gradient echo (SPGR) images: repetition time (TR) = 28 ms, echo time (TE) = 8 ms, flip angle = 40°, slice thickness = 1 mm, number of excitations (NEX) = 3, matrix = 256 × 192, field of view (FOV) = 16 × 16 cm. SPGR scans were taken consecutively throughout the infusion. T2-weighted images were acquired prior to and following infusions: TR = 2500 ms, TE = 110 ms, echo train length = 29, slice thickness = 2 mm, NEX = 4, matrix 256 × 224, FOV = 16 × 16 cm. The number of slices varied depending on the location and extent of the infusions (50–70 slices), and scan time varied from 13 to 15 minutes. Stereotactic coordinates for the target implant sites were determined from MR images. Rostral/caudal coordinates were determined based on linear (vegetable oil) reference markers located within the ear bars. Medial/lateral and dorsal/ventral coordinates were measured directly from bone landmarks on MR images that included the external sagittal crest and skull surface.

Stereotactic Frame/CED Infusion

Anesthetized dogs were placed in an MRI compatible stereotactic primate head frame that was modified by the addition of a bite plate holder. Components of the frame were constructed of either Plexiglass, aluminum, or brass. A dental impression mold was made for each animal in situ with vinyl polysiloxane impression material putty, (Express™ STD, 3 M ESPE Dental Products, St Paul, Minnesota) and the dogs' heads were stabilized with the bite plate and ear bars (Fig. 1).

The infusion cannula system consisted of four components (Fig. 1): (i) a 12-mm diameter (27 hole) or 8-mm diameter (6 hole) cylindrical plastic guide pedestal (Plastics One, Inc., Roanoke, Virginia), (ii) a fused silica infusion cannula consisting of a 22-gauge outer cannula with a 28-gauge inner cannula that was 2 mm longer than the outer guide cannula resulting in a stepped design, (iii) a sterile teflon loading line (0.508 mm inner diameter) containing the liposomes (Upchurch Scientific, Oak Harbor, Washington), and (iv) a nonsterile infusion line containing olive oil (Upchurch Scientific). On the basis of MRI coordinates, each guide pedestal was mounted onto a stereotactic arm (David Kopf Instruments, Tujunga, California) attached to the head frame, and manually guided to the targeted region of brain through burr holes made in the skull after sterile surgical exposure of the pedestal insertion site. The guide pedestals were secured to the skull with brass screws and ultraviolet curing urethane dimethacrylate gel (Triad Gel®, Dentsply International Inc., York, Pennsylvania). All guide pedestals were left in place for the duration of the treatment, thereby permitting repeated infusions. After infusions, the surgical site was closed over the guide pedestals that were sealed with plastic screw caps. All dogs received intraoperative antibiotics (Cephazolin 22 mg/kg, IV, q 4 hours) and a postoperative 2 week course of oral antibiotics (Cephalexin 22 mg/kg, PO, q 12 hours).

CED infusions were done by previously established techniques.[40,41] Briefly, dogs were placed in the MRI scanner; then infusion cannulae were inserted and secured after attachment of drug loading and infusion lines. Infusion pressure was generated by a 1-ml syringe loaded with oil and mounted on a microinfusion pump

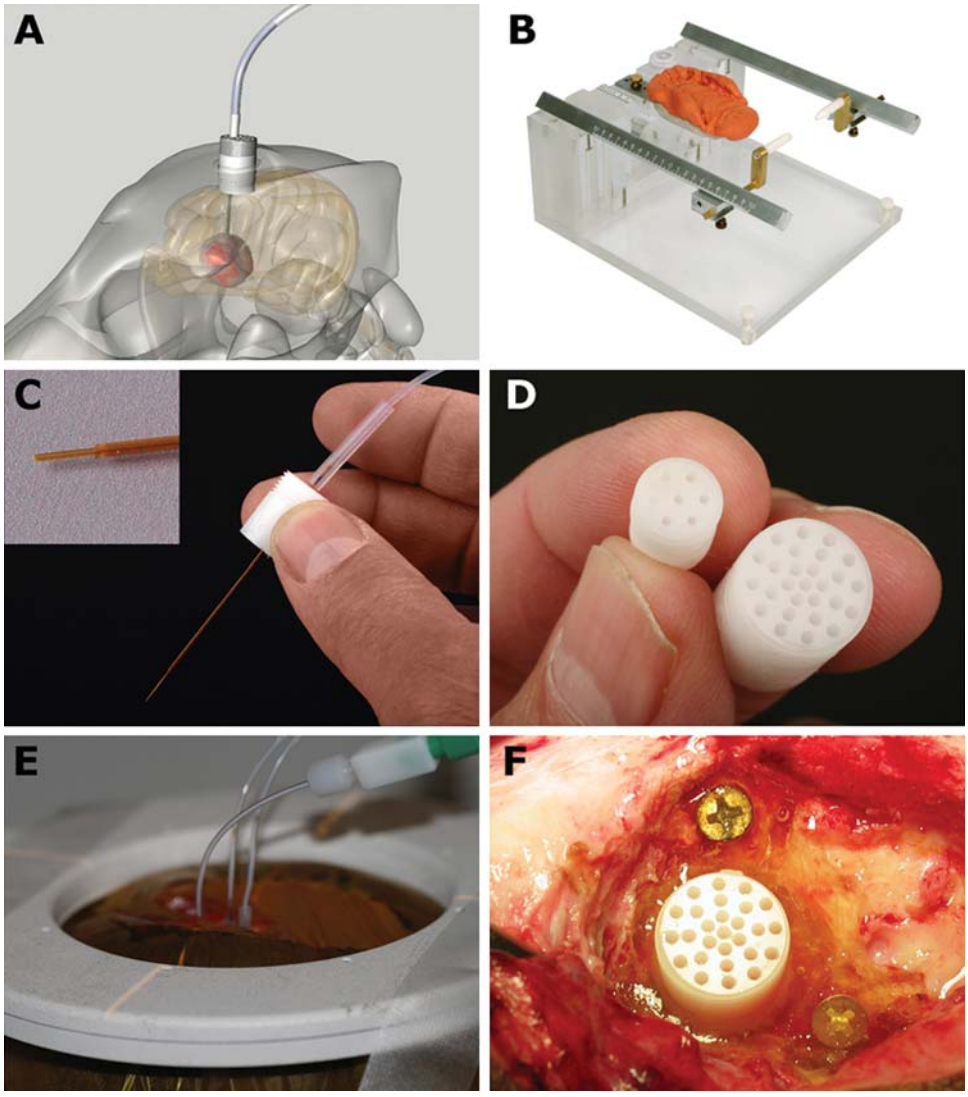

Fig. 1. Convection-enhanced delivery equipment used in the canine model system. (A) Schematic representation of indwelling guide pedestal system. (B) MRI compatible head frame utilizing ear bars and a dental bite plate. (C) Fused silica infusion cannulae with a reflux resistant step design are directed into the tumor site through the stereotactically placed guide pedestals. (D) Guide pedestals contain multiple ports to allow modification of targeting coordinates within the tumor. (E) Simultaneous infusion of liposomal infusate through 3 infusion cannulae. (F) Guide pedestals are secured *in situ* using rapid curing urethane dimethacrylate.

(BeeHive^{TM}, Bioanalytical Systems, West Lafayette, Indiana) located outside of the scanner. Infusion rates were started at 0.1 μL/min, and increased at 10-minute intervals to 0.2, 0.5, 0.8, 1.0, 1.5, 2.0, 2.5 μL/min and then to a maximum of 5.0 μL/min. Up to 4 individual infusion cannulae were used for each CED infusion procedure depending on the size of the tumor and placement of guide pedestals. Infusion procedures were repeated based on evidence of increasing tumor volume (or poor infusions with subsequent poor response) determined by serial MRI at 6–8-week intervals.

Volume Quantification

The volume of the tumors and infusate distribution (Vd) within tumor regions was determined using 3D image analysis software (OsiriX v.3.1, OsiriX Imaging Software, Osirix Foundation, Geneva, Switzerland). Briefly, tumor volumes were defined from T2-weighted MRI, and infusate distribution was defined based on T1-weighted SPGR images. Regions of interest (ROIs) were defined manually for individual contiguous MR image slices and volumes calculated with ROI volume software.

Neuropathological Examination

After euthanasia, brains were immersed in 10% buffered formalin for 7 days, sectioned transversely into 3-mm thick sections, and gross lesions were digitally photographed. Selected tissues were processed for routine paraffin embedding and then 5-μm thick sections were routinely stained with hematoxylin and eosin (HE) and Luxol-fast blue–HE (LFB–HE). Selected sections were also

immunostained by a modified streptavidin–biotin unlabeled immunoperoxidase technique with amino-ethyl-carbazide as the chromogen, essentially as described previously.[42] The polyclonal or monoclonal mouse antibodies used included a standard panel for canine cell-specific immunophenotypic markers, including CD3, CD18, CD45, CD 79a, as well as for CD20, CD31, Factor VIII RA, GFAP, caspase 3, triple neurofilament protein, synaptophysin, and Neu-N with antibody dilutions, pretreatments, and positive controls, as described previously.[42] The tumor proliferative index (in %) was calculated from MIB-1 immunoreactivity. All canine gliomas from both the initial CT-guided biopsy and at necropsy were histologically classified and graded according to the criteria established for the human WHO 2007 classification of tumors of the CNS.[43]

Results

Nine dogs with intra-axial gliomas (1 grade II astrocytoma, 3 anaplastic astrocytomas, 2 oligodendrogliomas, 3 anaplastic oligodendrogliomas) were infused with liposomal CPT-11/Gadoteridol. Signalment and infusion summaries are presented in Table 1. Total infusion times ranged from 135 to 290 minutes. The maximum total infusion volume (administered between 3 catheters) during a single procedure was 2.125 mL.

Tumor Volume/Infusion Volumes

One to four infusion cannulae per dog were used to infuse the tumors (Fig. 1), and direct infusion into nonresected tumors was achieved in all cases. All infusions were monitored approximately every 15 minutes by MRI. The infusions lasted from 1 to 4 hours, and the total volume of infusate varied from less than 50 μL to approximately 2 mL. Tumor volumes were considered to be well defined on T2-weighted MR images in 7 of 8 dogs. Dog 3 had extensive T2-signal changes after treatment, which made assessment of tumor volumes unreliable, and this animal was excluded from volume and distribution analysis. The distribution of tumor determined by MRI correlated well with histopathological tissue sections at necropsy in all dogs except Dog 3.

The range of maximal tumor volumes for the dogs was 1.29–7.13 cm^3 (mean 4.0 cm^3, median 3.6 cm^3, SD 2.3 cm^3). Infusate distribution volumes (Vd) and percentage coverage of tumor volumes were calculated for a total of 27 infusion procedures. Vd varied considerably both between infusion procedures and between individual catheters within a procedure. The range of total percentage coverage for individual procedures was 0.02–90% (mean 38%, median 28%, SD 23%).

The clinical effect of the infusions in tumors responsive to CPT-11 chemotherapy assessed by repeat MRI and histopathology was subjectively correlated with the Vd determined by real-time imaging during the infusion procedure (Figs 2–4). Poor infusions with early leakage and poor Vd resulted in minimal changes in tumor volume or imaging characteristics (Fig. 3), whereas infusions with increasing Vd and percent coverage of the tumor volume resulted in an apparent reduction in tumor volume, necrosis, and decreased or static tumor growth.

Leakage

The most common limitation in the procedure was the leakage of infusate into low pressure systems such as a ventricle or subarachnoid space (Figs 2, 3, and 6), which resulted in a poor volume of distribution within the target tissue, as previously described.[44] Leakage into necrotic cavities resulting from previous infusions, as well as into adjacent normal brain structures such as the internal capsule was also documented (Figs 4 and 6). The reflux of infusate along the cannula track was uncommon unless infusion rates exceeded 5 μL/min. Infusion rates >5 μL/min were only used once Vd had reached a plateau following leakage into a low pressure system (Figs 2, 3, and 6). Once leakage had occurred, a further increase in Vd was negligible regardless of infusion rate.

Table 1. Clinical case signalment

Patient	Breed/sex	Age (y)	Tumor type/grade	Survival (d)[b]	No. CED infusions	Cause of death
1	Jack Russell terrier FS	9	Astrocytoma II/III[a]	+331	3	Euthanasia (hemangiosarcoma)[c]
2	Boxer M	8	Astrocytoma II/III[a]	+560	6	Euthanasia (tumor progression)
3	French bulldog FS	10	Astrocytoma II/III[a]	+363	3	Euthanasia (tumor progression)
4	Labrador MC	10	Astrocytoma II	+190	3	Euthanasia (pancreatitis)[c]
5	Boston terrier MC	6	Oligodendroglioma II	+126	1	Died (status epilepticus)[c]
6	Boxer MC	7	Oligodendroglioma III	+147	2	Euthanasia (tumor progression)
7	English bulldog MC	5	Oligodendroglioma III	+190	3	Euthanasia (tumor progression)
8	Labrador FS	14	Oligodendroglioma II	+611	3	Alive
9	Boston terrier M	6	Oligodendroglioma III	+181	2	Alive

[a]Initial grade based on streotactic/CT biopsy; final grade based on necropsy.
[b]Survival was determined from the time of initial MRI diagnosis.
[c]Cause of death was determined to be unrelated to tumor progression.

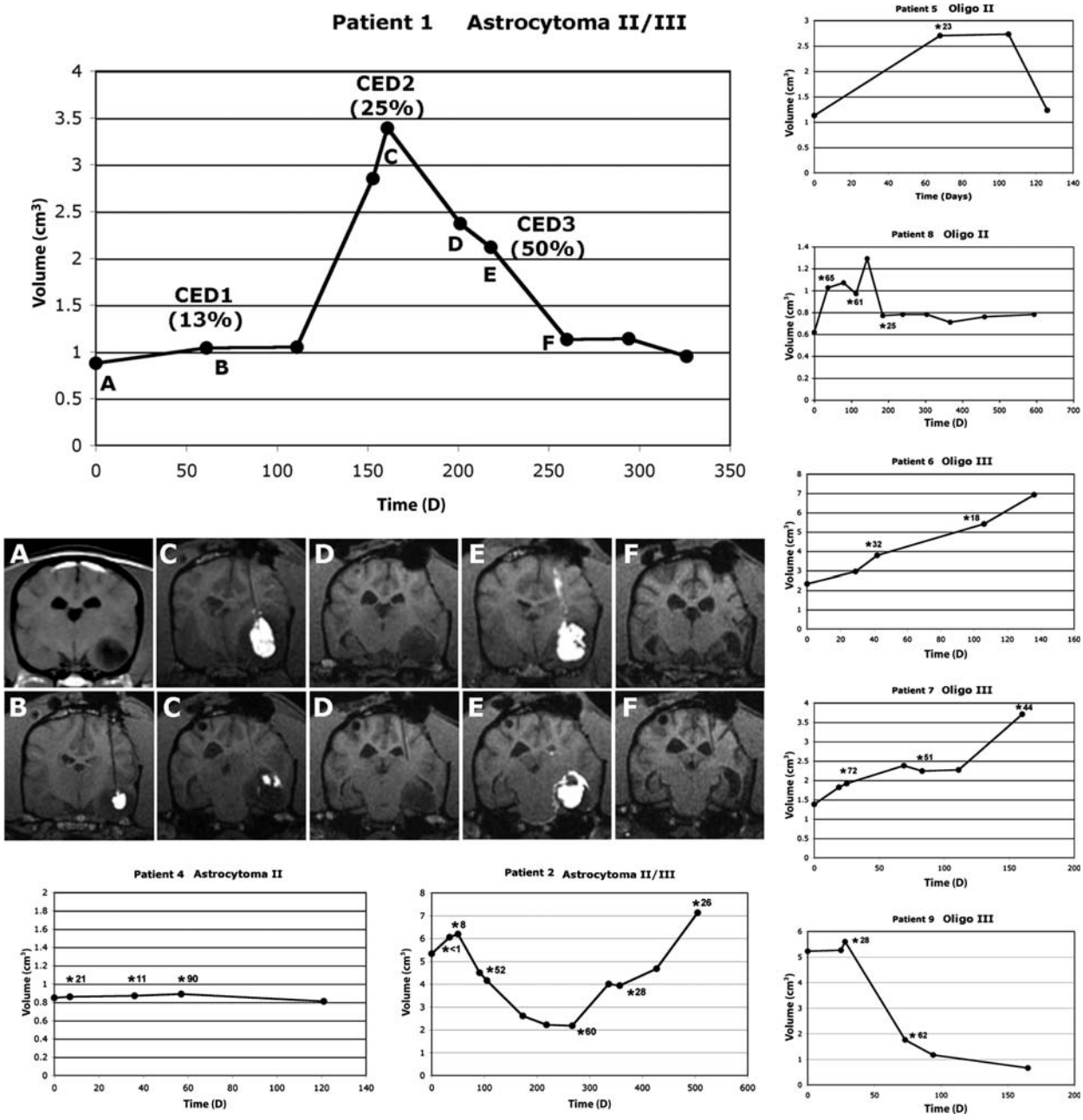

Fig. 2. Patient tumor volumes following intratumoral CED of liposomal CPT-11. CED infusions are represented by asterisks, with total percentage of tumor coverage for each infusion. Patient 1 is shown with associated MR imaging. MR images (T1 weighted) correlate to therapeutic or monitoring time points represented graphically. Real-time monitoring of infusions defined appropriate targeting and volume of distribution critical for objective assessment of therapeutic efficacy. (A) Initial MR imaging and tumor volume. (B) Initial single cannula infusion resulting in 13% Vd within the tumor and subsequent minimal effect on tumor growth. (C) Rapid tumor growth was followed by a second infusion, resulting in 25% Vd within the tumor and a subsequent decrease in tumor volume (D). (E) Third infusion, using two cannulae, resulted in 55% Vd within the tumor. A dramatic decrease in tumor volume was seen (F) followed by static disease before the animal was euthanized for disease unrelated to the primary tumor. Reflux of infusate (E, upper panel) and leakage into ventricles and the subarachnoid space (E, lower panel) were clearly visible on imaging, and dictated eventual infusion termination to minimize potential toxicity. In this apparently chemosensitive tumor, increasing real-time defined volume of distribution was associated with increasing response based on tumor volume.

Clinical/MRI Response

Maximum percentage decrease in tumor volume following therapy was 88% with 5 tumors having a decrease of 40% or greater (2 grade III astrocytomas 65%, 72%; 2 grade II oligodendrogliomas 40%, 55%; 1 grade III oligodendroglioma 88%). One grade II astrocytoma (Dog 4) was considered to have static disease. Two

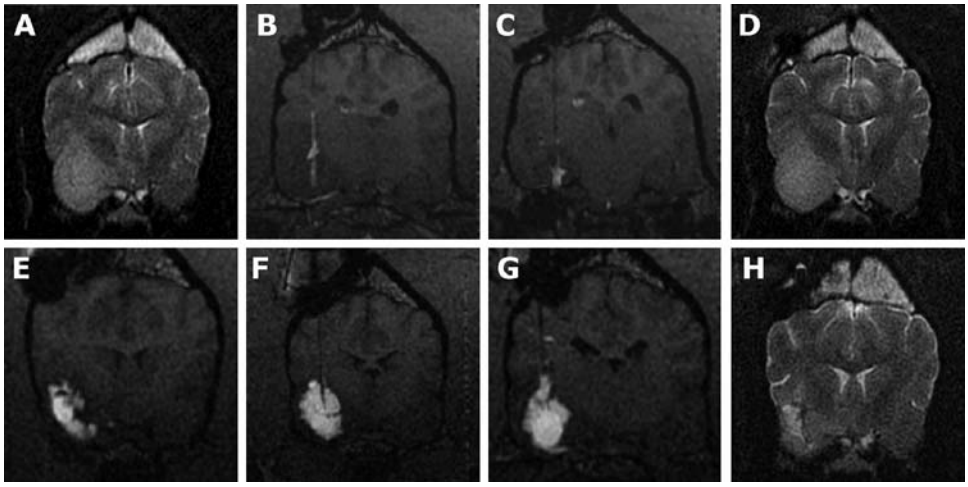

Fig. 3. MR images from a Boxer with a grade III astrocytoma. (A) Initial diagnostic MRI; the temporal/pyriform lobe tumor is most easily seen on T2-weighted images. (B and C) T1-weighted real-time images during two separate infusions (2 weeks apart) showing poor Vd within the tumor because of leakage into the subarachnoid space and lateral ventricle. Documented poor Vd was associated with minimal effect of tumor volume (D). Repositioning of guide pedestals to target different sites within the tumor resulted in improved Vd (>50%) using 3 infusion cannulae (E, F, G, T1-weighted images). (H) T2-weighted image 2 months following the successful infusion; improved Vd is associated with a decrease in tumor volume with associated decreased mass effect (an area of malacia is present within the tumor and the ipsilateral sulci and lateral ventricle are more prominent).

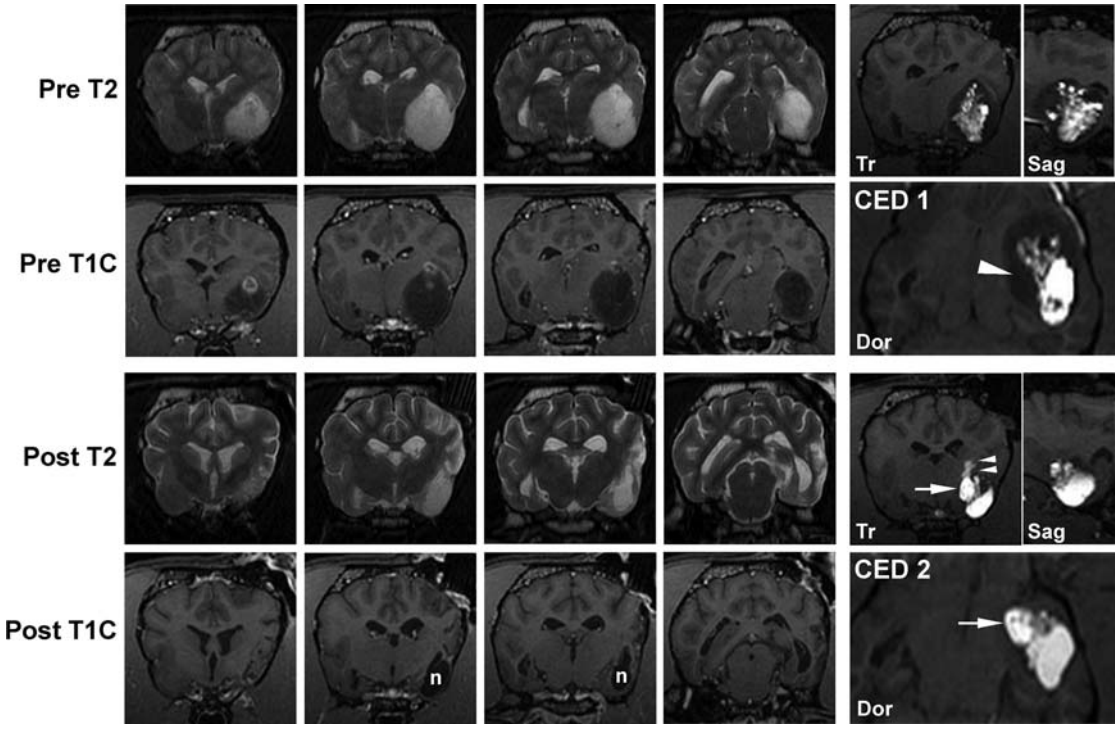

Fig. 4. MR images from a Boston Terrier with a grade III oliogdendroglioma. Two infusion procedures (CED 1,2) achieved 28% and 62% Vd, respectively, within the tumor, resulting in an 88% total reduction in tumor volume 5 months following initial treatment. Decreased tumor volume, decreased mass effect, and presumed necrosis (*n*) of the tumor is seen on posttreatment MR images. Real-time imaging of the first CED procedure identified poor coverage of the medial aspect of the mass (arrow head). An infusion cannula was specifically targeted to this area in the second procedure resulting in good medial coverage (arrows). Suboptimal placement of this cannula superficially within the tumor eventually resulted in leakage into the internal capsule (double arrow heads). Real-time imaging allowed detection and termination of the infusion to limit potential toxicity. Tr, transverse plane image; Sag, sagittal plane image; Dor, dorsal plane image.

dogs (Dogs 1 and 8) had static disease after an initial decrease in tumor volume. Dog 1 had no increase in tumor volume for 2 months and was euthanized for an unrelated disease. Dog 8 is alive and has had no increase in tumor volume for 14 months. Dog 9 is alive 6 months post diagnosis with an 88% reduction in tumor volume. No apparent response to therapy was seen in 2 anaplastic grade III oligodendrogliomas.

Adverse Events

Cannula placement and infusion procedures were tolerated well by all patients except Dog 3. Animals were reported by the owners to appear quieter for 4–5 days after infusions, but returned to preinfusion activity levels thereafter. Dog 3 had prolonged anesthetic recovery after the initial infusion and had a decreased neurological status 8 weeks after treatment. MRI revealed ipsilateral diffuse white and grey matter hyperintensity on T2-weighted imaging consistent with vasogenic and cytotoxic edema. Both MRI abnormalities and clinical signs were responsive to corticosteroid therapy (prednisolone 0.5 mg/kg BID [Fig. 6]). Dog 8 had a mild decrease in neurological status 2 weeks after the second CED procedure associated with ipsilateral-increased T2 signal predominantly involving white matter that was also rapidly responsive to corticosteroid therapy.

CSF was collected sequentially from 8 dogs, and a mild, predominantly lymphocytic pleocytosis (range 4–158 total nuleated cells/μL; reference <3/μL) was seen in 5 dogs. Seven of 9 dogs received anti-inflammatory doses of corticosteroids either for peritumoral edema present prior to treatment or following MRI evidence of posttreatment edema or CSF pleocytosis.

Pathology

A total of 7 brain tumors were evaluated after necropsy and assigned into 1 of 2 groups. Within the first group (5 dogs), lesions were present within tumors corresponding to sites of prior intratumoral CPT-11 infusion, based on infusion MR images. In these tumors (3 grade III astrocytomas, 1 grade II astrocytoma, 1 grade II oligodendroglioma) were variably sized areas of cystic malacia and intratumoral necrosis corresponding to sites of previous infusions (Figs 2, 3, and 5; Table 2). Immediately adjacent to this malacia, a zone of change in the tumor cell cytomorphology and pattern compared with that of the untreated tumor cell type was present in the 3 grade III astrocytomas and grade II oligodendroglioma (Fig. 5). In the astrocytomas, the modified GFAP-immunoreactive astrocytoma cells were much less dense, more uniformly spindloid, and with a proliferative index 15-fold lower (12–15% vs <1%) than the untreated areas of tumor. Although each of these tumors had been classified as grade II astrocytoma based on the initial stereotactic biopsy, there were now in all tumors substantial areas of untreated tumor, which were now classified as grade III. The grade II

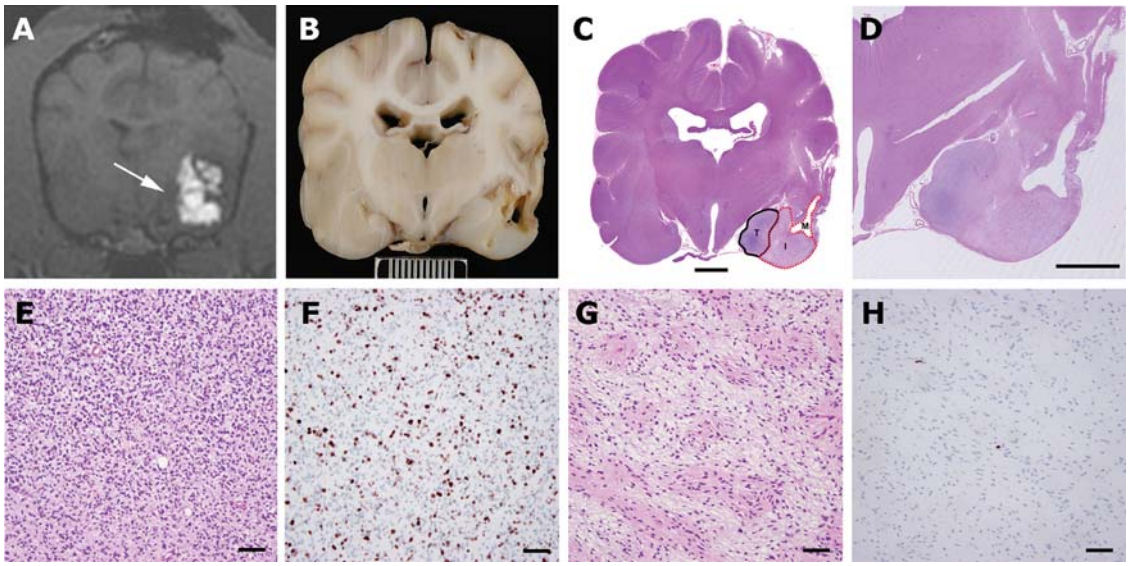

Fig. 5. Necropsy data from Patient 1. Real-time imaging of infusions and availability of necropsy in all clinical cases allowed histopathological data to be correlated with areas of infused and noninfused tumor and normal brain. (A) T1-weighted real-time imaging of the final CED showing poor infusion of tumor tissue medially (arrow). (B) Gross pathological specimen at the same level as the MRI (scale bar = 1 cm). (C) Whole brain section (hematoxylin and eosin) showing distinct areas consisting of infused tumor with malacia (M), infused tumor with modified tumor (I), and noninfused tumor (T) (scale bar = 500 μm). (D) Magnified view of infusion area (hematoxylin and eosin, scale bar = 500 μm). Modification of tumor phenotype was seen in areas of tumor that were infused (G, hematoxylin and eosin) compared with noninfused tumor (E, hematoxylin and eosin). Infused tumor was less cellular with a more homogenous cellular phenotype. MIB-1 index in infused tumor (H) was <1% compared with 15% in noninfused tumor (E) (E, F, G, H, sacle bar = 60 μm).

Table 2. Pathology summary

Patient no.	Tumor type/grade	Tumoral necrosis	Modified phenotype	MIB-1 decrease (infused tumor)	Adverse reaction[a]
1	Astrocytoma II/III	++	++	15% → <1%	−
2	Astrocytoma II/III	++	++	12% → <1%	−
3	Astrocytoma II/III	+	++	14% → <1%	++
4	Astrocytoma II	++	−	−	−
5	Oligodendroglioma II	++	+	4% → <1%	−
6	Oligodendroglioma III	−	−	−	−
7	Oligodendroglioma III	−	−	−	−
8	Oligodendroglioma II	+	ND	ND	+
9	Oligodendroglioma III	++	ND	ND	−

Abbreviation: ND, not done.
[a]Adverse reactions were defined by diffuse T2W hyperintensity beyond the margins of the tumor or infusion, not present on pretreatment MRI. Both adverse reactions were associated with decreased neurological status.

oligodendroglioma (Dog 5) had a large area of cystic malacia, also surrounded by cytologically modified tumor cells (GFAP immunonegative) exhibiting a much lower proliferative index (4% vs <1%) than the noninfused tumor. In the grade II astrocyoma (Dog 4), there was a small area of cystic malacia surrounded only by the same original grade II astrocytoma in the untreated area.

Dog 3 (grade III astrocytoma) was categorized as having an adverse reaction to the CPT-11 infusion. The tumor had an area of cystic malacia, again with more peripheral phenotypically modified astrocytoma cells and with multiple sites of an expansive and aggressive grade III astrocytoma. Additionally, outside of the tumor were widespread areas of encephalomalacia restricted to the shrunken left hemisphere and compatible in location with the adverse postinfusion response detected on MRI (Fig. 6).

In the second group of 2 high-grade (III) oligodendrogliomas, there were no apparent gross or microscopic lesions corresponding to the sites of infusion.

Within all tumors, and peritumorally, there was almost no detectable inflammatory cell response, suggesting the essential safety of CED and that the liposomal CPT-11/Gd does not evoke any detrimental toxicity apart from targeted tumor necrosis.

Discussion

Direct delivery and liposomal encapsulation of CPT-11 have been shown to decrease local toxicity and allow much higher concentrations of drug to be achieved at the target site compared with either systemic or free drug delivery.[39,45] The efficacy of liposomal topoisomerase inhibitors delivered by CED in rodent glioma models has been previously documented,[39,45–47] as has our ability to monitor CED infusions by co-infusion of liposomes containing gadolinium as a surrogate marker.[37,48] We have also previously demonstrated that CED of liposomally encapsulated CPT-11 and gadoteridol results in negligible clinical and histopathological adverse effects in normal experimental dogs,[40] and the current study suggests that this is also true for dogs with intra-axial gliomas. Although most animals exhibited mild lymphocytic pleocytosis in CSF analyzed after infusions, only 2 animals showed evidence of either histopathological or MRI changes consistent with an adverse reaction to the infusion. Both animals exhibited a deterioration in neurological status and both were rapidly responsive to corticosteroids (Fig. 5; Table 2); although marked atrophy/malacia involving both grey and white matter was seen in the most severely affected animal (Dog 3). While marked leakage of infusate into nontargeted peritumoral tissues was documented in this case, T2W hyperintensity in the second dog (Dog 8) occurred after infusions that were essentially limited to the tumor volume, and leakage of infusate in other animals was not associated with apparent adverse effects. The likelihood of adverse effects secondary to inappropriate targeting of liposomes to normal brain or CSF were minimized, since real-time imaging allowed for the termination of infusions, alteration of infusion rates, and/or redirection of infusion cannulae when leakage, distribution to normal brain, or static volumes of distribution were documented during the infusion process.

Although assessment of therapeutic efficacy was not a defined endpoint for the study, evidence for efficacy of intratumoral liposomal CPT-11 in these spontaneous tumors and indications of its potential mechanism of action were apparent in the study animals. The natural biology of canine spontaneous gliomas is poorly documented, as is response to conventional therapy such as radiation and chemotherapy. The endpoint for most animals is euthanasia rather than overall survival, and published "survival" data range from several days to several months for all treatment options. As such, any efficacy of direct intratumoral infusion of liposomal CPT-11 could only be assessed subjectively for individual cases on the basis of MRI evidence of static or decreasing tumor volumes and histopathology after euthanasia or death. Liposomal encapsulation has been shown to improve the pharmacokinetic properties and tissue residence time of CPT-11, which has been detected in rodent glioma models up to 2 months after a single CED administration.[39,45] Consistent with this experimental data, the efficacy of treatment in dogs

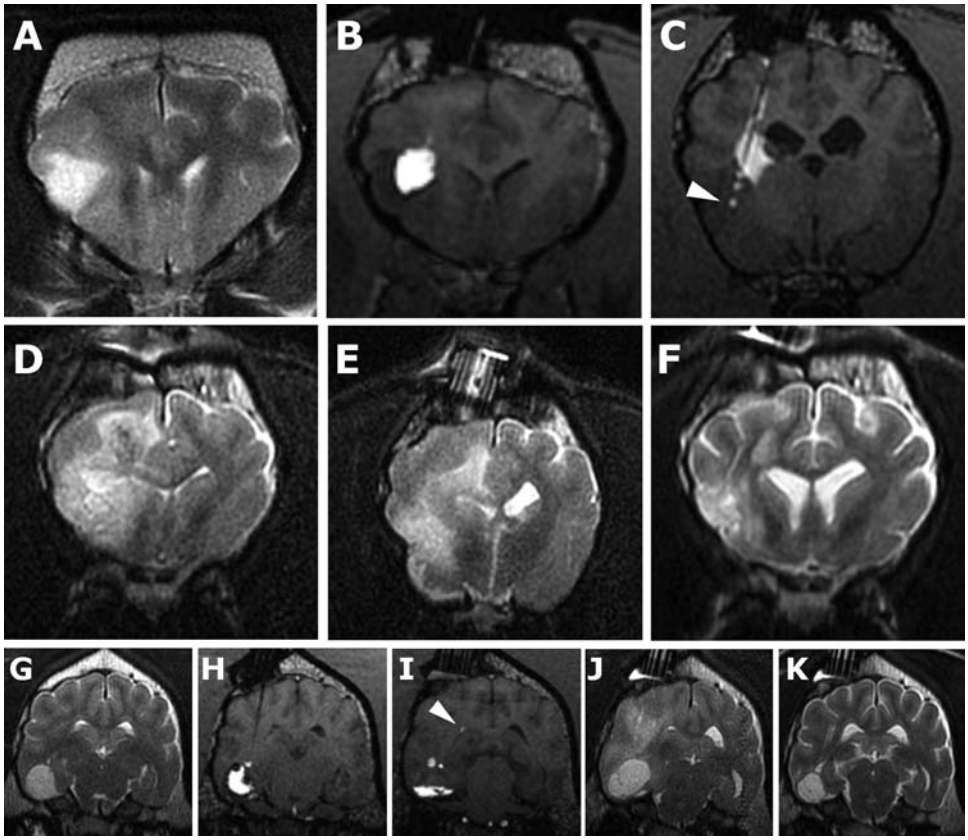

Fig. 6. Adverse effects associated with nanoliposomal CPT-11/gadoteridol infusions. (Patient 3, A–F; Patient 8, G–K.) (A) Preinfusion T2W MR image. (B and C) CED using 3 cannulae resulted in intratumoral delivery rostrally; however, reflux of infusate from the caudal cannula resulted in delivery into the internal capsule instead of the target site (arrowhead). (D and E) T2W MR images 8 weeks postinfusion; T2 hyperintensity is present predominantly affecting white matter, resulting in ventricular compression and effacement of sulci. (F) T2W MR image 6 weeks later following corticosteroid treatment with resolution of the majority of the white matter hyperintensity. (G) Preinfusion T2W MR image. First (H) and second (I) infusions (T1W MR images). The first infusion achieved good intratumoral Vd, whereas the second was restricted to the ventral aspect of the tumor. Both infusions were eventually limited by ventricular leakage (arrowhead). (J) Four weeks postinfusion, clinical deterioration was associated with T2 hyperintensity predominantly associated with white matter and also increased tumor volume. (K) Four weeks following corticosteroid treatment and rapid resolution of clinical signs, T2 hyperintensity and associated mass effect has resolved, and tumor volume is decreased.

receiving multiple infusions appeared to be present over several weeks, based on serial MRI (Fig. 2).

Five tumors decreased in volume ranging from 40% to 88%, and 1 dog with grade II astrocytoma (Dog 4) had apparently stable disease (Fig. 2). The small area of malacia present within this tumor was probably because of expansion of the CT-biopsy cavity since pooling of infusate was noted in this area during treatments. Malacia secondary to toxic effects in infused neuropil was considered less likely because this was not a finding in other cases or in previous experimental dogs.[40] Two tumors, both anaplastic oligodendrogliomas, had rapid growth progression and had no apparent response based either on MRI or histopathology. Importantly, the lack of response in these tumors was associated with successful intratumoral infusions, as defined by real-time imaging (Fig. 2). The percent coverage of tumor determined by real-time imaging varied from 32% to 72%, a degree of coverage associated with apparent positive responses in other tumors. These cases, therefore, suggested that there was a true failure of the therapeutic drug rather than a failure of the delivery system. In contrast, the lack of response in Dog 2 (grade III astrocytoma) after the initial 2 infusions was clearly associated with poor Vd secondary to leakage and tumor coverage of $<10\%$ (Figs 2 and 3). Subsequent delivery of liposomal CPT-11 covering $>50\%$ of this tumor resulted in a marked decrease in tumor volume. Similar findings were apparent in Patient 1 (grade III astrocytoma) where limited infusions covering approximately 10% of tumor volume had only slight clinical effect compared with subsequent infusions where tumor coverage was 25% or greater (Fig. 2). Although the number of dogs in the study was small and tumor phenotype varied, the critical value of real-time imaging in defining Vd of infusions and subsequent assessment of therapeutic efficacy of a novel therapeutic delivered by CED is clearly demonstrated, as are the potential pitfalls of assessing therapeutic value in the absence of imaging.

The mechanism for the decreased sensitivity and lack of response in the 2 anaplastic oligodendrogliomas is

unclear. CPT-11, (7-ethyl-10-(4-[1-piperidinio]-1-piperidinio) carbonyloxycamptothecin) is a water-soluble derivative of the potent alkaloid anticancer agent camptothecin and acts as a specific inhibitor of topoisomerase I.[34] CPT-11 is converted into a more active metabolite, SN-38 (7-ethyl-10-hydroxycamptothecin), by carboxylesterase (CES) activity, predominantly in the liver and serum.[49] The precise contribution of SN-38 to the antineoplastic effect of CPT-11 compared with Irinotecan hydrochloride is unclear, as is the necessity for systemic metabolism. Some data suggest that intratumoral or neuropil activation of Irinotecan might be as important as systemic/hepatic activation and is an important factor when considering direct intratumoral infusion.[50–60] One of the largest decreases in tumor volume (~90%) following therapy was seen in the third anaplastic oligodendroglioma, suggesting, not surprisingly, that factors influencing therapeutic efficacy are not consistent across individual tumors of similar histological type and grade. Further investigation of factors such as carboxylesterase and topoisomerase expression in individual treated tumors may be more informative regarding the sensitivity when tumor infusion has been documented by MRI.

A major advantage of the canine spontaneous tumor model is the availability of necropsy (all nonsurviving animals in this study), providing valuable correlative data often unavailable from human clinical trials. Two major responses were noted in tumors examined histopathologically: necrosis and a modulation of the tumor phenotype. Consistent with the predictive value of real-time imaging in relation to clinical response, histological findings after necropsy were also closely correlated with real-time infusion images. Overlay of MR infusion images and histological sections showed areas of tumor necrosis and/or modulation of tumor phenotype in areas of infused tumor, with residual/new tumor present beyond the margins of infusion exhibiting a more aggressive phenotype (Fig. 5). Modulation of tumor phenotype was seen in 4 of 5 necropsied animals that displayed a decreased tumor volume or static disease. Modulation was characterized by more benign, less anaplastic cellular characteristics, and a decrease in the MIB-1 proliferative index (Fig. 5; Table 2). The mechanism for this altered phenotype following exposure to CPT-11 is unclear, but may involve selective targeting of a more proliferative compartment of tumor cells, leaving terminally differentiated tumor cells as a residual population. The authors have also seen this tumor modulation after CED of liposomal CPT-11 in orthotopic murine tumor models with a canine glioma cell line. The presence of essentially nondividing, yet apparently viable, tumor tissue after therapy has important implications for both the prognosis and assessment of efficacy simply measured in terms of reduction in tumor volume. Routine MRI did not discriminate between untreated tumor and tumor with modified phenotype, and additional imaging approaches such as diffusion-weighted imaging and spectroscopy may be beneficial in defining this modified compartment of the tumor.

In summary, we have shown that canine spontaneous gliomas may provide a valuable large animal, spontaneous tumor model for the investigation of novel delivery, and novel therapeutic strategies for intracranial tumors. It is hoped that retrospective analysis of MRI parameters and infusion data in this more clinically realistic spontaneous model may help to further optimize cannula and infusion parameters. CED of a chemotherapeutic agent (liposomal CPT-11) directly into spontaneous gliomas in a large volume brain is feasible and well tolerated clinically. On the basis of responses in canine patients, intratumoral liposomal CPT-11 should be considered as a potential therapeutic option, particularly in nonresectable or recurrent tumors. As was the case with these spontaneous gliomas in dogs, assessment and optimization of any therapy delivered by CED in future human glioma clinical trials will depend critically on the ability to accurately define infusions in real time. In addition to providing an appropriate mechanistic and biological environment to assess CED parameters more realistically, the canine model has provided an equally realistic system to assess potential adverse effects associated with the infusion procedure, the delivery system, therapeutic agent, and surrogate marker in the context of a large immunocompetent mammal with ongoing intracranial disease.

Conflict of interest statement. D.B.K., C.O.N., and D.C.D. both hold stock and stock options in Merrimack Pharmaceuticals, the company working to develop this novel drug formulation. D.B.K. was previously the Vice President of Pharmaceutical Research and Development for Hermes Biosciences, a company working to develop the product that was recently merged with Merrimack Pharmaceuticals. D.B.K. and D.C.P. are the inventors on a patent application that describes the highly stabilized nanoliposome formulation of CPT-11 used in this manuscript. D.C.P. is the Senior Director of Research for Merrimack Pharmaceuticals. J.W.P. is a Board member, officer in Hermes Biosciences, Inc. and also has equity in the same company. The University of California–San Francisco has a patent related to this work.

Funding

This work was supported by the National Institutes of Health [1PO1 CA-118816-0102 and P50 CA097257] and The Paul C. and Borghild T. Petersen Foundation.

References

1. Fomchenko EI, Holland EC. Mouse models of brain tumors and their applications in preclinical trials. *Clin Cancer Res*. 2006;12:5288–5297.
2. Branle F, Lefranc F, Camby I, et al. Evaluation of the efficiency of chemotherapy in *in vivo* orthotopic models of human glioma cells with and without 1p19q deletions and in C6 rat orthotopic allografts serving for the evaluation of surgery combined with chemotherapy. *Cancer*. 2002;95:641–655.
3. Vail DM, MacEwen EG. Spontaneously occurring tumors of companion animals as models for human cancer. *Cancer Invest*. 2000;18:781–792.
4. Koestner A, Bilzer T, Fatzer R, Schulman FY, Summers BA, Van Winkle TJ. Histological Classification of Tumors of the Nervous System of Domestic Animals. 2nd ed, vol. 5. Washington, D.C: The Armed Forces Institute of Pathology; 1999.
5. Paoloni M, Khanna C. Translation of new cancer treatments from pet dogs to humans. *Nat Rev Cancer*. 2008;8:147–156.
6. Kimmelman J, Nalbantoglu J. Faithful companions: a proposal for neurooncology trials in pet dogs. *Cancer Res*. 2007;67:4541–4544.
7. Surawicz TS, McCarthy BJ, Kupelian V, Jukich PJ, Bruner JM, Davis FG. Descriptive epidemiology of primary brain and CNS tumors: results from the Central Brain Tumor Registry of the United States, 1990–1994. *Neuro Oncol*. 1999;1:14–25.
8. McKinney PA. Brain tumours: incidence, survival, and aetiology. *J Neurol Neurosurg Psychiatry*. 2004;75(suppl 2):ii12–ii17.
9. Klotz M. Incidence of brain tumors in patients hospitalized for chronic mental disorders. *Psychiatr Q*. 1957;31:669–680.
10. McGrath JT. Intracranial pathology of the dog. *Acta Neuropathol (Berl)*. 1962;1(suppl I):3–4.
11. Schneider R. General considerations. In: Moulton, JE ed. Tumors in Domestic Animals. 2nd ed. Berkley: University of California Press; 1978:1–15.
12. Priester WA, McKay FW. The occurrence of tumors in domestic animals. In: Ziegler, JL ed. National Cancer Institute Monograph. Bethseda, MD: U.S. Department of Health and Human Services; 1980:1–210.
13. Candolfi M, Curtin JF, Nichols WS, et al. Intracranial glioblastoma models in preclinical neuro-oncology: neuropathological characterization and tumor progression. *J Neurooncol*. 2007;85:133–148.
14. Summers BA, Cummings JF, de Lahunta A. Tumors of the Central Nervous System. Veterinary Neuropathology St Louis: Mosby; 1995:351–401.
15. Vandevelde M, Fankhauser R, Luginbühl H. Immunocytochemical studies in canine neuroectodermal brain tumors. *Acta Neuropathol (Berl)*. 1985;66:111–116.
16. Sturges BK, Dickinson PJ, Bollen AW, et al. Magnetic resonance imaging and histological classification of intracranial meningiomas in 112 dogs. *J Vet Intern Med*. 2008;22:586–595.
17. Stoica G, Kim HT, Hall DG, Coates JR. Morphology, immunohistochemistry, and genetic alterations in dog astrocytomas. *Vet Pathol*. 2004;41:10–19.
18. Westworth DR, Dickinson PJ, Vernau W, et al. Choroid plexus tumors in 56 dogs (1985–2007). *J Vet Intern Med*. 2008;22:1157–1165.
19. Snyder JM, Shofer FS, Van Winkle TJ, Massicotte C. Canine intracranial primary neoplasia: 173 cases (1986–2003). *J Vet Intern Med*. 2006;20:669–675.
20. Thomas WB, Wheeler SJ, Robert K, Kornegay JN. Magnetic resonance imaging features of primary brain tumors in dogs. *Vet Radiol Ultrasound*. 1996;37:20–27.
21. Kraft SL, Gavin PR, DeHaan C, Moore M, Wendling LR, Leathers CW. Retrospective review of 50 canine intracranial tumors evaluated by magnetic resonance imaging. *J Vet Intern Med*. 1997;11:218–225.
22. Lipsitz D, Higgins RJ, Kortz GD, Dickinson PJ, Bollen AW, LeCouteur RA. Glioblastoma multiforme: clinical findings, magnetic resonance imaging and pathology in 5 dogs. *Vet Pathol*. 2003;40:659–669.
23. Dickinson PJ, Roberts BN, Higgins RJ, et al. Expression of receptor tyrosine kinases VEGFR-1 (FLT-1), VEGFR-2 (KDR), EGFR-1, PDGFRα and c-Met in canine primary brain tumors. *Vet Comp Oncol*. 2006;4:132–140.
24. Dickinson PJ, Sturges BK, Higgins RJ, et al. Vascular endothelial growth factor mRNA expression and peritumoral edema in canine primary central nervous system tumors. *Vet Pathol*. 2008;45:131–139.
25. Debinski W, Gibo DM, Wykosky J, Stanton C, Rossmeisl J, Robertson J. Canine gliomas over-express IL-13Ralpha2, EphA2 and Fra-1 in common with human high-grade astrocytomas. *Neuro Oncol*. 2007;9:535.
26. Stoica G, Lungu G, Stoica H, Waghela S, Levine J, Smith R, 3rd. Identification of cancer stem cells in dog glioblastoma. *Vet Pathol*. 2009;
27. Thomson SA, Kennerly E, Olby N, et al. Microarray analysis of differentially expressed genes of primary tumors in the canine central nervous system. *Vet Pathol*. 2005;42:550–558.
28. Platt SR, Scase TJ, Adams V, et al. Vascular endothelial growth factor expression in canine intracranial meningiomas and association with patient survival. *J Vet Intern Med*. 2006;20:663–668.
29. Long S, Argyle DJ, Nixon C, et al. Telomerase reverse transcriptase (TERT) expression and proliferation in canine brain tumours. *Neuropathol Appl Neurobiol*. 2006;32:662–673.
30. Thomas R, Duke SE, Wang HJ, et al. 'Putting our heads together': insights into genomic conservation between human and canine intracranial tumors. *J Neurooncol*. 2009;94:333–349.
31. Higgins RJ, Dickinson PJ, Lecouteur RA, et al. Spontaneous canine gliomas: overexpression of EGFR, PDGFRalpha and IGFBP2 demonstrated by tissue microarray immunophenotyping [published online ahead of print December 5, 2009]. *J Neurooncol*. 2009.
32. Dickinson PJ, Surace EI, Cambell M, et al. Expression of the tumor suppressor genes NF2, 4.1B, and TSLC1 in canine meningiomas. *Vet Pathol*. 2009;46:884–892.
33. Debinski W, Tatter SB. Convection-enhanced delivery for the treatment of brain tumors. *Expert Rev Neurother*. 2009;9:1519–1527.
34. Potmesil M. Camptothecins: from bench research to hospital wards. *Cancer Res*. 1994;54:1431–1439.
35. Hare CB, Elion GB, Houghton PJ, et al. Therapeutic efficacy of the topoisomerase I inhibitor 7–ethyl-10-(4-[1-piperidino]-1-piperidino)-carbonyloxy-camptothecin against pediatric and adult central nervous system tumor xenografts. *Cancer Chemother Pharmacol*. 1997;39:187–191.
36. Feun L, Savaraj N. Topoisomerase I inhibitors for the treatment of brain tumors. *Expert Rev Anticancer Ther*. 2008;8:707–716.
37. Saito R, Krauze MT, Bringas JR, et al. Gadolinium-loaded liposomes allow for real-time magnetic resonance imaging of convection-enhanced delivery in the primate brain. *Exp Neurol*. 2005;196:381–389.
38. Krauze MT, McKnight TR, Yamashita Y, et al. Real-time visualization and characterization of liposomal delivery into the monkey brain by magnetic resonance imaging. *Brain Res Brain Res Protoc*. 2005;16:20–26.
39. Noble CO, Krauze MT, Drummond DC, et al. Novel nanoliposomal CPT-11 infused by convection-enhanced delivery in intracranial tumors: pharmacology and efficacy. *Cancer Res*. 2006;66:2801–2806.

40. Dickinson PJ, LeCouteur RA, Higgins RJ, et al. Canine model of convection-enhanced delivery of liposomes containing CPT-11 monitored with real-time magnetic resonance imaging: laboratory investigation. *J Neurosurg*. 2008;108:989–998.
41. Bankiewicz KS, Eberling JL, Kohutnicka M, et al. Convection-enhanced delivery of AAV vector in parkinsonian monkeys; *in vivo* detection of gene expression and restoration of dopaminergic function using pro-drug approach. *Exp Neurol*. 2000;164:2–14.
42. Higgins RJ, LeCouteur RA, Vernau KM, Sturges BK, Obradovich JE, Bollen AW. Granular cell tumor of the canine central nervous system: two cases. *Vet Pathol*. 2001;38:620–627.
43. Louis DN, Ohgaki H, Wiestler OD, Cavenee WK. WHO classification of tumors of the central nervous system. 4th ed. Geneva: WHO Press; 2007.
44. Varenika V, Dickinson P, Bringas J, et al. Detection of infusate leakage in the brain using real-time imaging of convection-enhanced delivery. *J Neurosurg*. 2008;109:874–880.
45. Krauze MT, Noble CO, Kawaguchi T, et al. Convection-enhanced delivery of nanoliposomal CPT-11 (irinotecan) and PEGylated liposomal doxorubicin (Doxil) in rodent intracranial brain tumor xenografts. *Neuro Oncol*. 2007;9:393–403.
46. Saito R, Krauze MT, Noble CO, et al. Convection-enhanced delivery of Ls-TPT enables an effective, continuous, low-dose chemotherapy against malignant glioma xenograft model. *Neuro-oncology*. 2006;8: 205–214.
47. Yamashita Y, Krauze MT, Kawaguchi T, et al. Convection-enhanced delivery of a topoisomerase I inhibitor (nanoliposomal topotecan) and a topoisomerase II inhibitor (pegylated liposomal doxorubicin) in intracranial brain tumor xenografts. *Neuro-oncology*. 2007; 9:20–28.
48. Saito R, Bringas JR, McKnight TR, et al. Distribution of liposomes into brain and rat brain tumor models by convection-enhanced delivery monitored with magnetic resonance imaging. *Cancer Res*. 2004;64: 2572–2579.
49. Kaneda N, Nagata H, Furuta T, Yokokura T. Metabolism and pharmacokinetics of the camptothecin analogue CPT-11 in the mouse. *Cancer Res*. 1990;50:1715–1720.
50. Atsumi R, Okazaki O, Hakusui H. Metabolism of irinotecan to SN-38 in a tissue-isolated tumor model. *Biol Pharm Bull*. 1995;18:1024–1026.
51. Guichard S, Terret C, Hennebelle I, et al. CPT-11 converting carboxylesterase and topoisomerase activities in tumour and normal colon and liver tissues. *Br J Cancer*. 1999;80:364–370.
52. Kawato Y, Furuta T, Aonuma M, Yasuoka M, Yokokura T, Matsumoto K. Antitumor activity of a camptothecin derivative, CPT-11, against human tumor xenografts in nude mice. *Cancer Chemother Pharmacol*. 1991;28:192–198.
53. Ohtsuka K, Inoue S, Kameyama M, et al. Intracellular conversion of irinotecan to its active form, SN-38, by native carboxylesterase in human non-small cell lung cancer. *Lung Cancer*. 2003;41:187–198.
54. Nagai S, Yamauchi M, Andoh T, et al. Establishment and characterization of human gastric and colonic xenograft lines resistant to CPT-11 (a new derivative of camptothecin). *J Surg Oncol*. 1995;59:116–124.
55. Niimi S, Nakagawa K, Sugimoto Y, et al. Mechanism of cross-resistance to a camptothecin analogue (CPT-11) in a human ovarian cancer cell line selected by cisplatin. *Cancer Res*. 1992;52:328–333.
56. Hu ZP, Yang XX, Chen X, Chan E, Duan W, Zhou SF. Simultaneous determination of irinotecan (CPT-11) and SN-38 in tissue culture media and cancer cells by high performance liquid chromatography: application to cellular metabolism and accumulation studies. *J Chromatogr B Analyt Technol Biomed Life Sci*. 2007;850:575–580.
57. Sanghani SP, Quinney SK, Fredenburg TB, et al. Carboxylesterases expressed in human colon tumor tissue and their role in CPT-11 hydrolysis. *Clin Cancer Res*. 2003;9:4983–4991.
58. Zhang W, Xu G, McLeod HL. Comprehensive evaluation of carboxylesterase-2 expression in normal human tissues using tissue array analysis. *Appl Immunohistochem Mol Morphol*. 2002;10: 374–380.
59. Yamada T, Hosokawa M, Satoh T, et al. Immunohistochemistry with an antibody to human liver carboxylesterase in human brain tissues. *Brain Res*. 1994;658:163–167.
60. Furihata T, Hosokawa M, Satoh T, Chiba K. Synergistic role of specificity proteins and upstream stimulatory factor 1 in transactivation of the mouse carboxylesterase 2/microsomal acylcarnitine hydrolase gene promoter. *Biochem J*. 2004;384:101–110.